AIP Journal of Applied Physics

Dielectric, hypersonic, and domain anomalies of (PbMg 1/3 Nb 2/3 O 3) 1−x (PbTiO 3) x single crystals

Chi-Shun Tu, C.-L. Tsai, V. Hugo Schmidt, Haosu Luo, and Zhiwen Yin

Citation: Journal of Applied Physics **89**, 7908 (2001); doi: 10.1063/1.1370998
View online: http://dx.doi.org/10.1063/1.1370998
View Table of Contents: http://scitation.aip.org/content/aip/journal/jap/89/12?ver=pdfcov
Published by the AIP Publishing

Dielectric, hypersonic, and domain anomalies of $(PbMg_{1/3}Nb_{2/3}O_3)_{1-x}(PbTiO_3)_x$ single crystals

Chi-Shun Tu[a] and C.-L. Tsai
Department of Physics, Fu Jen University, Taipei, Taiwan 242, Republic of China

V. Hugo Schmidt
Department of Physics, Montana State University, Bozeman, Montana 59717

Haosu Luo and Zhiwen Yin
Shanghai Institute of Ceramics, Chinese Academy of Sciences, Shanghai 201800, People's Republic of China

(Received 2 January 2001; accepted for publication 16 March 2001)

Dielectric permittivities, Brillouin backscattering spectra, polarization-electric field hysteresis loops, and domain structures have been measured as a function of temperature in relaxor-based ferroelectric single crystals $(PbMg_{1/3}Nb_{2/3}O_3)_{1-x}(PbTiO_3)_x$(PMN-$x$PT) for $x=0.24$ and 0.34. For PMN-24%PT, a diffuse phase transition which is associated with a broad frequency-dependent dielectric maximum was observed near 380 K. As the temperature increases, the PMN-24%PT crystal gradually develops cubic regions and is fully converted into the cubic state near 375 K. An extra dielectric anomaly appears at 370 K, possibly due to the percolating polar cluster induced by an external electric field. PMN-34%PT exhibits a nearly normal ferroelectric phase transition near 445 K from the tetragonal to the cubic phase. In addition, a weak diffuse phase transition observed near 280 K may result from partial conversion of rhombohedral phase to tetragonal phase. The dielectric thermal hysteresis confirms that the transitions near 280 and 445 K are diffuse first order and first order, respectively. The dielectric permittivities of PMN-24%PT and PMN-34%PT obey the relation, $\varepsilon_m'/\varepsilon'(f,T)=1+[T-T_m(f)]^{\gamma}/2\delta_{\gamma}^2$, above the temperature of permittivity maximum T_m. © *2001 American Institute of Physics.* [DOI: 10.1063/1.1370998]

I. INTRODUCTION

Relaxor ferroelectrics generally mean complex perovskites with and ABO_3-type unit cell and are crystals in which unlike-valence cations belonging to a given site (A or B) are presented in the correct ratio for charge balance, but are situated randomly on these cation sites.[1–4] These randomly different cation charges give rise to random fields, which tend to make the phase transitions ''diffuse'' instead of sharp as in normal ferroelectrics.[3,4] Lead–magnesium niobate, $Pb(Mg_{1/3}Nb_{2/3})O_3$ (PMN), is one of the most interesting relaxor ferroelectric (FE) materials. PMN has a disordered complex structure in which the Mg^{2+} and Nb^{5+} cations exhibit only short range order on the B site. Near 280 K the PMN crystal undergoes a diffuse phase transition characterized by a broad frequency-dependent dielectric maximum. PMN has cubic symmetry at room temperature with space group $Pm3m$, whereas below 200 K a small rhombohedral distortion (pseudocubic) was observed.[1,5] The normal FE crystal $PbTiO_3$ has tetragonal symmetry with space group $P4mm$ at room temperature and has a normal FE phase transition taking place at $T_c=760$ K with long-range FE order occurring below T_c.[6]

The relaxor-based FE crystals $(PbMg_{1/3}Nb_{2/3}O_3)_{1-x}(PbTiO_3)_x$(PMN-$x$PT) are expected to show properties of both relaxor ferroelectric PMN and normal ferroelectric PT. PMN-xPT naturally has a morphotropic phase boundary (MPB) in the range of ~28–~36 mol % of PT.[7] In other words, as the temperature decreases, the mixed crystals of PMN-xPT($0.28\leqslant x\leqslant 0.36$) have successive phase transitions: cubic paraelectric (PE) phase→tetragonal FE phase→rhombohedral FE phase. The spontaneous deformations of the tetragonal state appear along the equivalent ⟨001⟩ directions, giving six fully FE domain states with the spontaneous polarization P_s and the optical axes (OA) oriented parallel to ⟨001⟩. In the low temperature region, the crystals exhibit a polar rhombohedral phase with the P_s and the OA oriented along the ⟨111⟩ direction.

Paik *et al.* showed that a field of 20 kV/cm in PZN-8%PT destroys the rhombohedral state and induces a single tetragonal domain.[8] By *in situ* x-ray diffraction, Durbin *et al.* confirmed that the field-induced crystallographic change occurs.[9] By optical microscopy, with field applied along ⟨001⟩, Belegundu *et al.* confirmed that tetragonal and rhombohedral domains coexist at room temperature and even down to −100 °C.[10] Perhaps the strain caused by the presence of the eight ⟨111⟩-type domains is partly relieved by the presence of tetragonal ⟨001⟩ domains induced by the external dc field.

Single crystals of PMN-PT have been reported to exhibit much larger piezoelectric constants and electromechanical coupling factors compared with those in the $PbZrO_3-PbTiO_3$ (PZT) family of ceramics.[11–13] Such high piezoelectric performance, which converts mechanical and

[a]Author to whom correspondence should be addressed; electronic mail: phys1008@mails.fju.edu.tw

electric energies, is crucial in medical imaging, telecommunication, and ultrasonic devices and may revolutionize these applications.[14] Much work has been undertaken on the growth and characterization of relaxor-based ferroelectrics.[15–21] However, limited attention has been paid to phase transitions and domain structures in these crystals, especially phase coexistence near the MBP.[17,21] It is believed that the phase coexistence near the MPB plays an important role in the high electromechanical coupling effect. Therefore, we carried out temperature-dependent measurements of dielectric permittivity, Brillouin light scattering, $P-E$ hysteresis loops, and polarized light microscopy on PMN-24%PT and PMN-34%PT single crystals.

II. EXPERIMENTAL PROCEDURE

The lead magnesium niobate–lead titanate single crystals, PMN-24%PT and PMN-34%PT, were grown using a modified Bridgman method with bottom seed.[15] The samples were cut perpendicular to the {001} direction and were not electrically poled. Here, direction ''{}'' refers to the pseudocubic axes. For dielectric permittivities and $P-E$ hysteresis loops, the sample surfaces were coated with silver paste electrodes. The applied electric field was along the pseudocubic {001} direction. A variable-frequency Wayne–Kerr precision analyzer (PMA3260A) with four-lead connections was used to obtain capacitance and resistance. The heating/cooling rate for dielectric measurement was 1.5 K/min. For the field-cooled-zero-field-heated (FC-ZFH) dielectric measurement, the PMN-24%PT sample was first cooled from 470 K (cubic phase) to room temperature with a dc bias field of $E=6$ kV/cm along the {001} direction. Then the dielectric permittivity was measured upon heating without a bias field. The $P-E$ hysteresis loops were measured by using a Sawyer–Tower circuit in which the $P-E$ loop was obtained within two to four cycles of electric field at frequency of 47 Hz. A Janis CCS-450 closed cycle refrigerator was used with a LakeShore 340 temperature controller.

Longitudinal acoustic (LA) phonon spectra were obtained from the Brillouin backscattering. The samples were illuminated along the {001} direction with an Innova 90 plus-A3 argon laser with wavelength $\lambda=514.5$ nm. The transverse acoustic (TA) mode was not observed in this work. Scattered light was analyzed by a Burleigh five-pass Fabry–Pérot interferometer. The free spectral range of the Fabry–Pérot interferometer was determined by measuring the LA phonon shift of fused quartz. Due to the weak intensity factor and low optical transmission, the signal/noise (S/N) ratio of the LA phonon spectra is about 2–3 for both the PMN-24%PT and PMN-34%PT crystals, even though the S/N ratio from the fused quartz is greater than 60. The Brillouin scattering data were taken during a heating sequence.

The domain structures were studied by a Nikon E600POL polarized light microscope (PLM). The samples were cut perpendicular to the {001} direction and were finely polished. In order to minimize superposition of domains, the thickness of the samples is less than 65 μm. A Linkam THMS600 heating/cooling stage mounted on the microscope

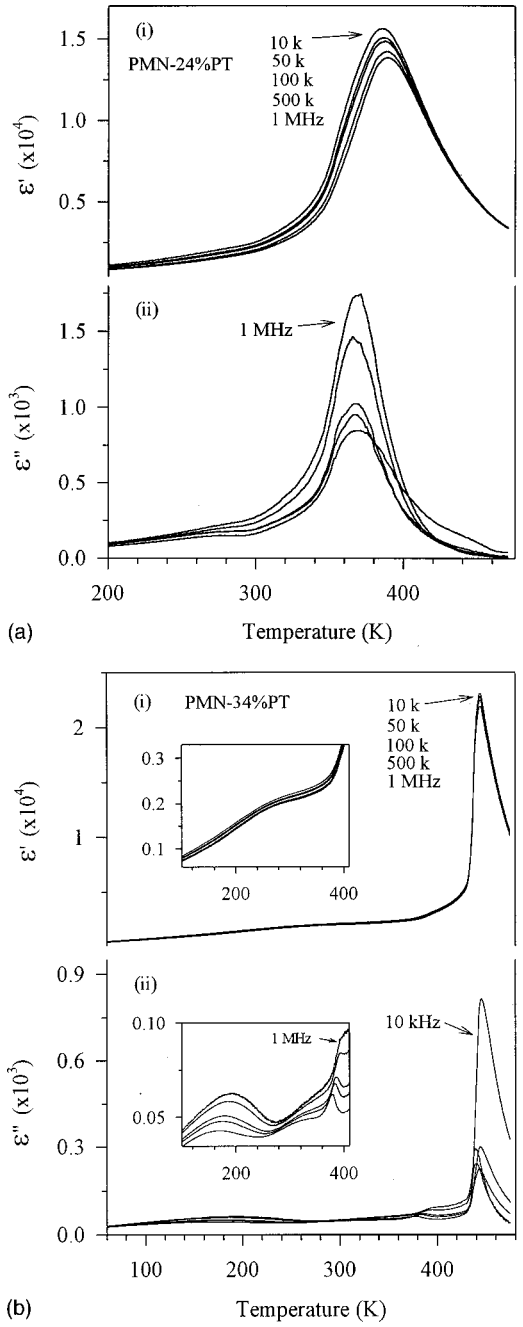

FIG. 1. Temperature dependences of (i) ε' and (ii) ε'' for (a) PMN-24%PT and (b) PMN-34%PT, obtained during a heating process. The insets are enlargements of ε' and ε''.

was used for studying domain structures as a function of temperature. Domain structures were observed between paralleled polarizer-analyzer along the {001} direction using a quarter-wave plate. In the tetragonal phase, adjacent domains are usually polarized 90° to each other and form strip-like domain walls.[22] Due to strain birefringence and total reflection at the boundary, the 90° domain wall is usually visible in the polarized light. In the rhombohedral phase, when observing the ⟨001⟩ cut of a platelet between crossed polarizers along the ⟨001⟩ direction, the cross section of the optical indicatrix will exhibit extinction directions parallel to the ⟨110⟩ equivalent directions.

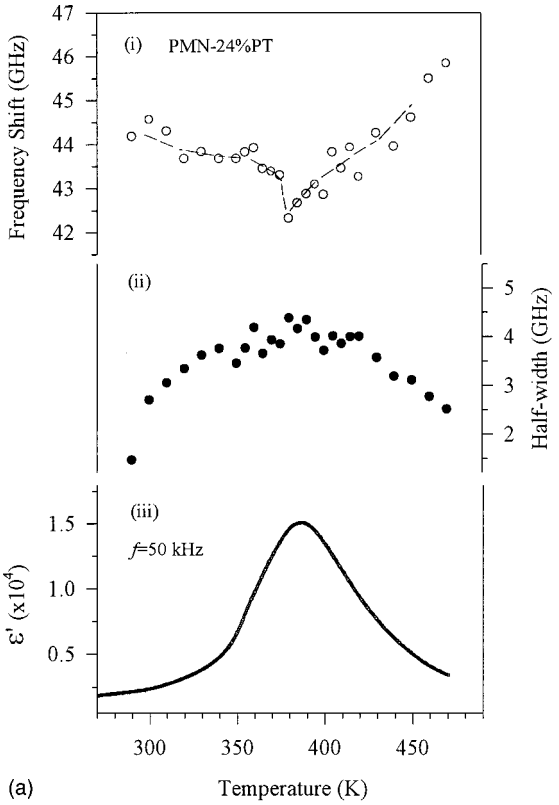

FIG. 2. (i) Brillouin frequency shift, (ii) half width, and (iii) ε' vs temperature for (a) PMN-24%PT and (b) PMN-34%PT. The dielectric data are taken at $f=50$ kHz upon heating. The dashed lines are guides for the eye.

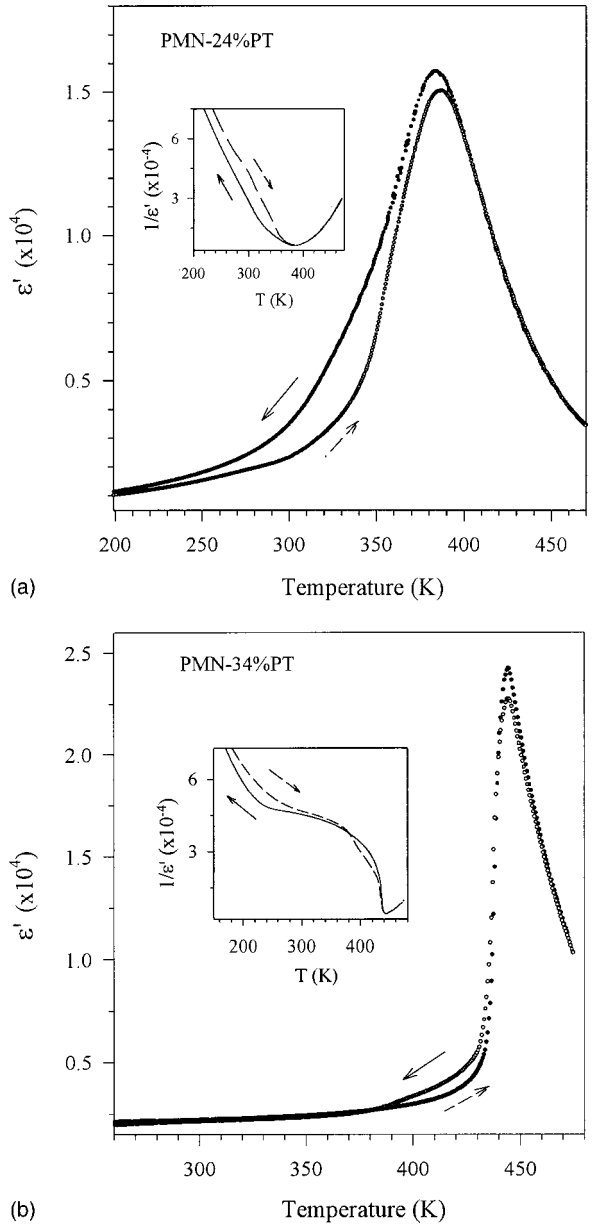

FIG. 3. Thermal hysteresis behavior of ε' for (a) PMN-24%PT and (b) PMN-34%PT, taken at $f=50$ kHz. The insets are the reciprocal of ε'.

III. EXPERIMENTAL RESULTS

Figures 1(a) and 1(b) show the temperature dependences of the real ε' and imaginary ε'' parts of the dielectric permittivity. The insets of Fig. 1(b) are enlargements of ε' and ε'' to clarify the dispersion behaviors which appear below 410 K. Compared with the prototypical relaxor PMN, the ε' of PMN-24%PT shows similar frequency-dependent behavior, with much higher values of $\varepsilon'_m \sim 1.5\times 10^4$ and $T_m \sim 380$ K. T_m corresponds to the temperature giving maximum value ϵ'_m of the dielectric permittivity. However, near 445 K the dielectric permittivity ϵ' of PMN-34%PT exhibits a nearly normal FE transition with very slight frequency dispersion. Both the values of $\varepsilon'_m \sim 2.3\times 10^4$ and $T_m \sim 445$ K of PMN-34%PT are greater than those in PMN and PMN-24%PT due to more PT content. In PMN-34%PT, ε' shows a broad weak plunge accompanied by a dispersion near room temperature, which may be connected to a diffuse phase transition of part of the crystal from the rhombohedral to the tetragonal phase. A sharper but weak frequency-dependent anomaly in the ε''

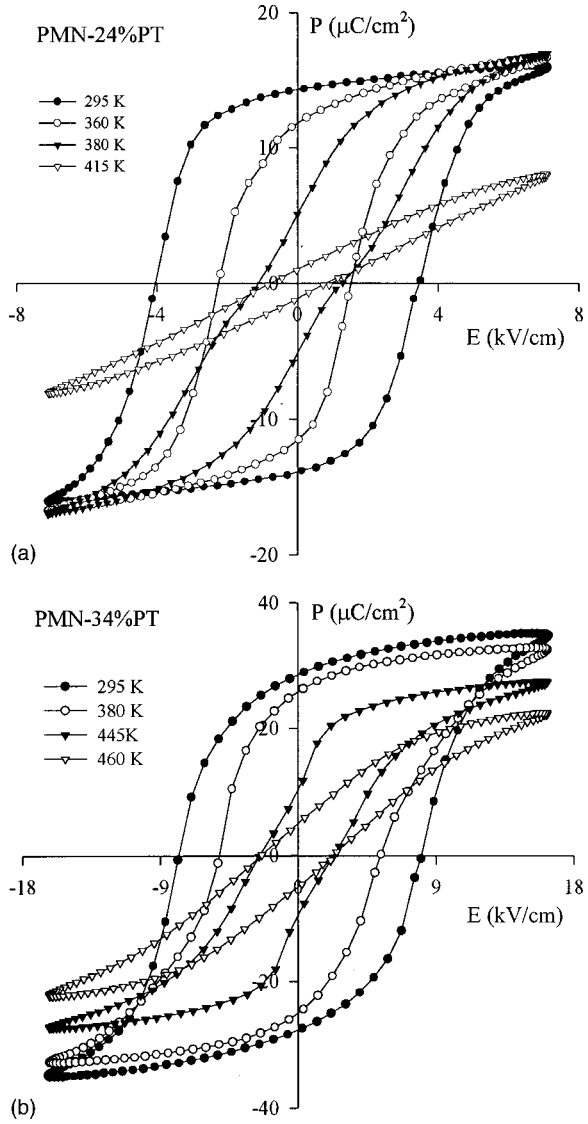

FIG. 4. $P-E$ hysteresis loops of (a) PMN-24%PT and (b) PMN-34%PT upon heating.

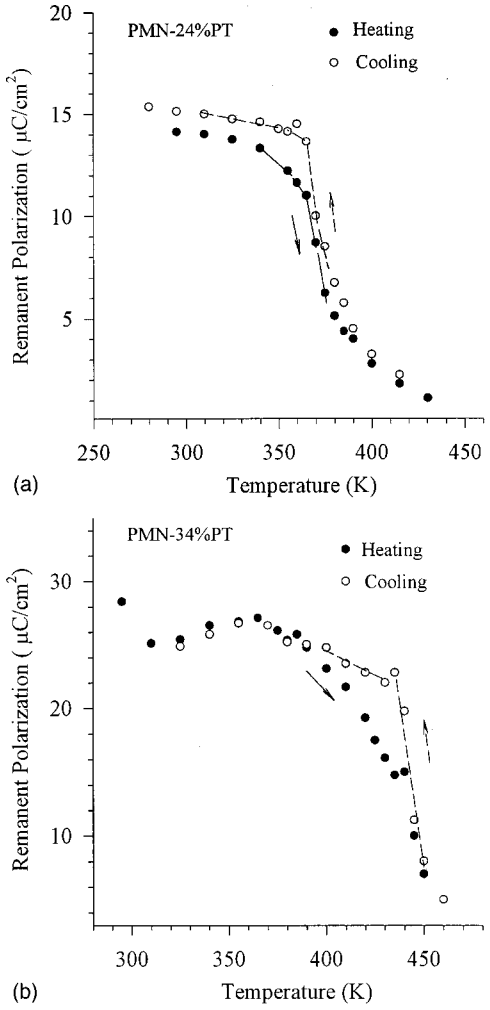

FIG. 5. Temperature dependence of P_r for (a) PMN-24%PT and (b) PMN-34%PT. The solid and dashed lines are guides for the eye.

data [Fig. 1(b)] was observed near 390 K and may result from partial conversion of rhombohedral phase to cubic phase.

Figures 2(a) and 2(b) show, respectively, the temperature dependences of the phonon frequency, half width, and dielectric permittivity ϵ'. As shown in Fig. 2(a), the acoustic phonon frequency of PMN-24%PT exhibits a broad minimum near 380 K, which corresponds to the broad dielectric maximum. The acoustic phonon frequency of PMN-34%PT [Fig. 2(b)] shows two successive minima near 280 and 445 K, respectively. Figures 3(a) and 3(b) show the temperature-dependent data of ε' from cooling and heating processes at measuring frequency $f=50$ kHz. The insets of Figs. 3(a) and 3(b) show the reciprocal behaviors of ϵ'. Below ~380 K PMN-24%PT exhibits a thermal hysteresis in a wide temperature range. For PMN-34%PT, two clear thermal hystereses were observed in the regions of ~150–300 and ~380–460 K. In particular, typical dielectric behavior of a first-order FE phase transition appears near 445 K.[23]

$P-E$ hysteresis loops are shown in Figs. 4(a) and 4(b). At room temperature, the remanent polarization P_r of PMN-24%PT is 15 μC/cm^2, and is about the same as the spontaneous polarizations P_s defined as the intercept at zero field of the straight-line portion of the hysteresis loop. By comparison, PMN-34%PT has P_r of 28 and P_s near 32.5, and PT has[24,25] P_s of 52 in these units. The coercive field E_c, however, is not monotonic with the PT content. It goes from 3.4 kV/cm for PMN-24%PT to 8.0 for PMN-34%PT, and is back down to 6.75 for PT.[24] We cannot explain this E_c dependence, but will discuss the P_s dependence on the PT content. If one would assume a linear dependence of P_s on the PT content, then P_s for PMN-24%PT would be about 30 μC/cm^2. This estimate assumes that the FE phase remains tetragonal. In reality, it consists of rhombohedral clusters near room temperature.[7] Accordingly, we assume that P_s has magnitude of 30 μC/cm^2 for each cluster, and that for large field along the $\langle 001\rangle$ the cluster polarizations lie in the four $\langle 111\rangle$ directions with a $+1$ component along c. Then the net P_s is along c and is reduced by the factor $1/\sqrt{3}$ to 17 μC/cm^2, which is close to the measured value of 15 μC/cm^2. The temperature-dependent behaviors of P_r are plotted in Figs. 5(a) and 5(b). Instead of a gradual temperature-dependent behavior of polarization as seen in PMN,[26] a sharp

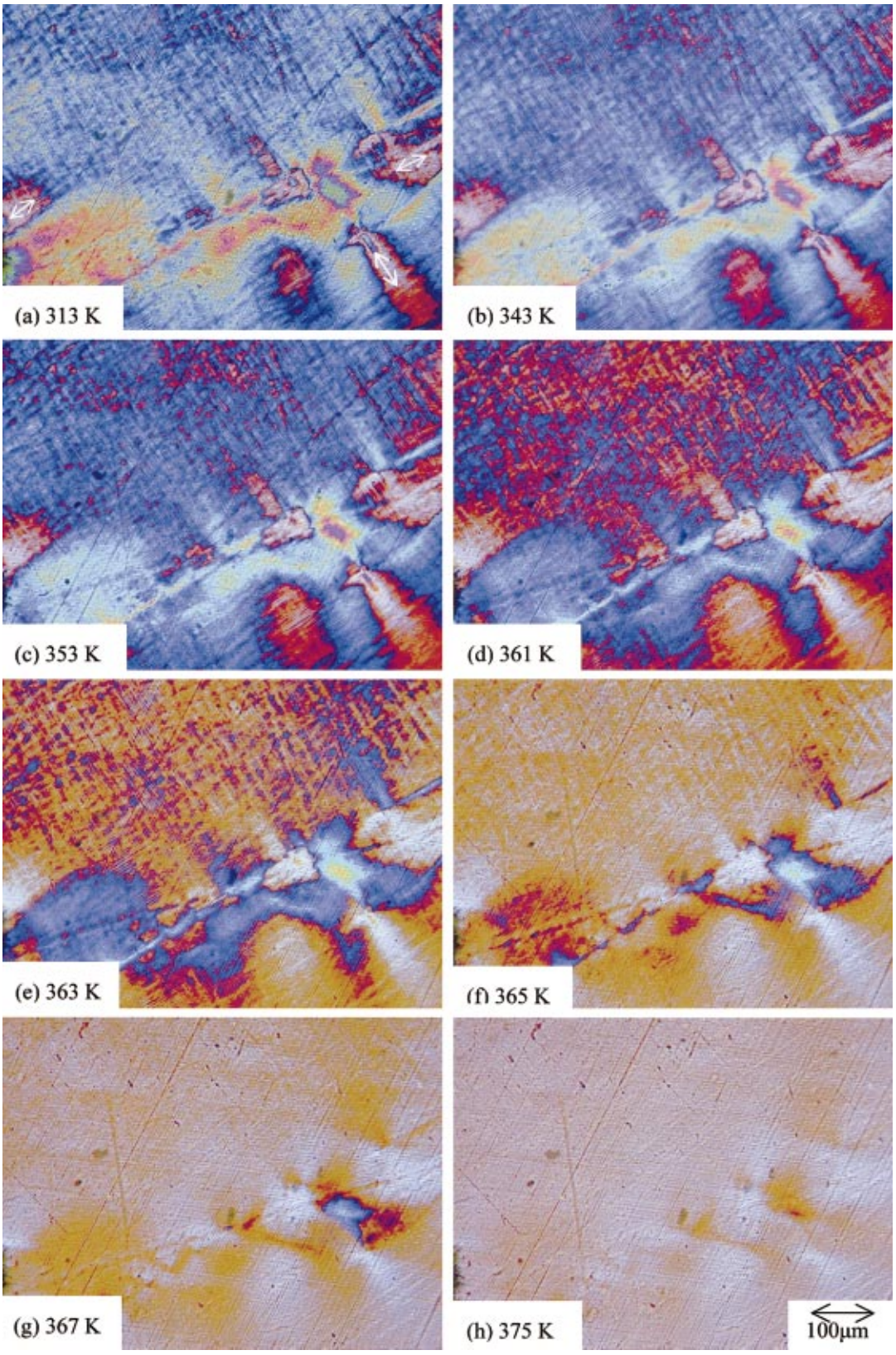

FIG. 6. (a) (Color) Successive domain structures of PMN-24%PT.

change was observed near 370 and 440 K for PMN-24%PT and PMN-34%PT, respectively. The thermal hysteresis behavior implies a metastable state near the phase transition temperature.[23]

Temperature-dependent domain structures are shown in Figs. 6(a) and 6(b). At lower temperature phase, the domain structures of PMN-24%PT exhibit complicated interference patterns probably caused mostly by clusters or microdomains

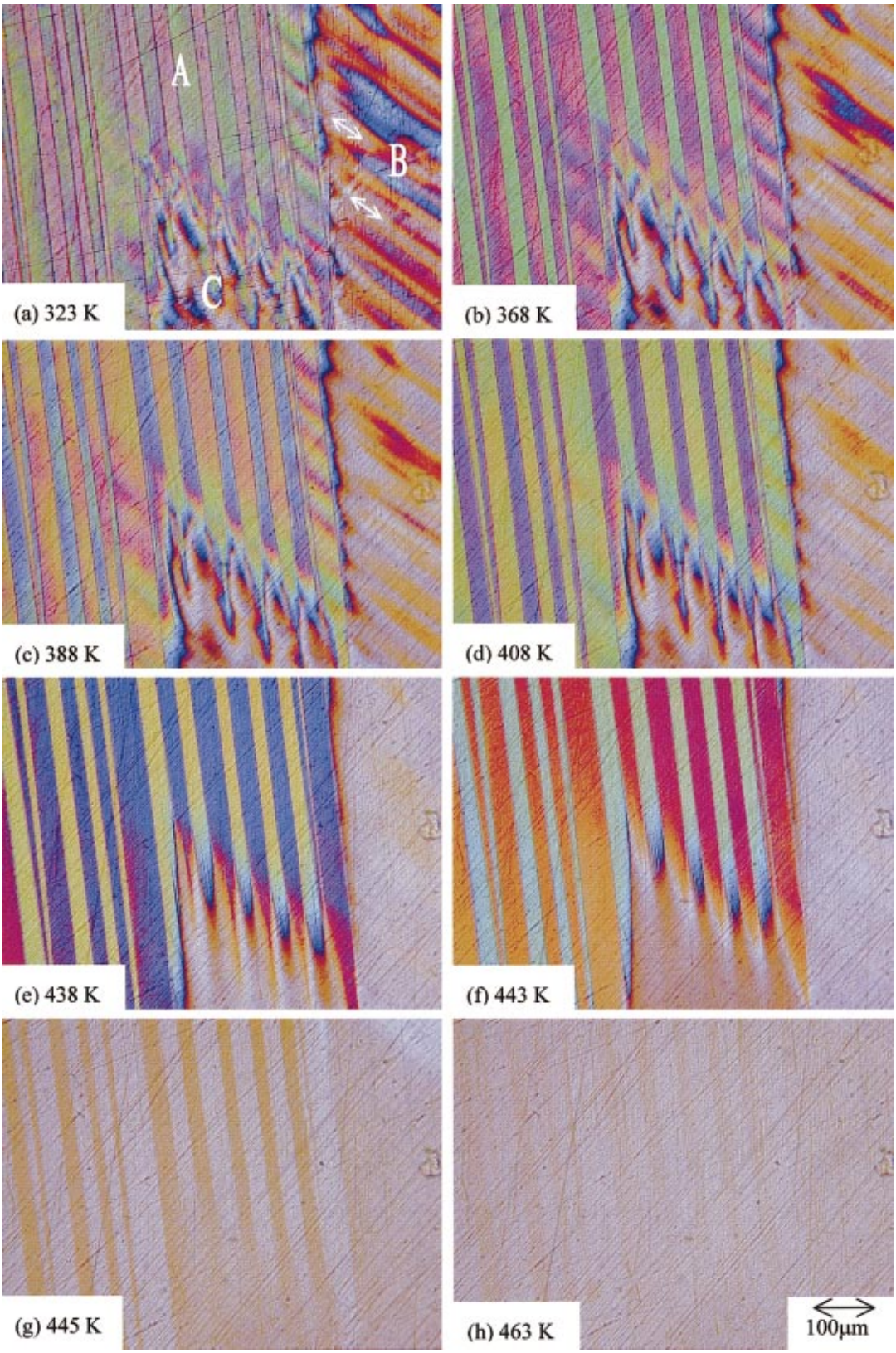

FIG. 6. (b) (Color) Successive domain structures PMN-34% PT..

but partly by domains. As shown in Fig. 6(a), those regions (indicated by arrows) which exhibit optically isotropic background color possibly correspond to rhombohedral (pseudocubic) clusters with the extinction directions along ⟨110⟩.[21] We expect a rhombohedral phase in these domain regions for two reasons. First, according to the MPB,[7] PMN-24%PT has only rhombohedral distortion near room temperature. Second, pure PMN crystal remains optically isotropic without formation of macrodomains and shows a pseudocubic symmetry down to very low temperature.[27] As

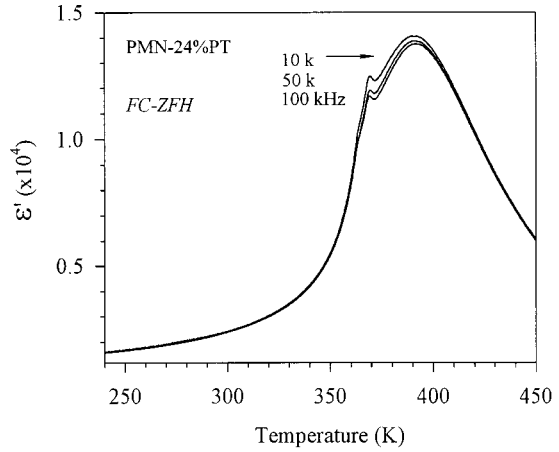

FIG. 7. Temperature dependence of ε' obtained from the FC-ZFH of PMN-24%PT.

the temperature increases, the domain structures gradually change and go completely into the optically isotropic cubic phase near 375 K. On the other hand, the rhombohedral state with interference color domains suggests that macrorange FE clusters have been triggered by the substitution of 24% Ti^{4+} for the *B* site complex ions $(Mg_{1/3}Nb_{2/3})^{4+}$. It is believed that the introduction of Ti^{4+} increases the size of local polar domains by strengthening the off-center displacement and enhances the interactions between micropolar domains, leading to macroscopic symmetry breaking of the pseudocubic state in small portions of the crystal.

The PMN-34%PT crystal corresponds to the MPB composition in the PMN-PT system, and is expected to have complex domain structures. As shown in the ''(a)'' pattern of Fig. 6(b), domain structures of PMN-34%PT can be distinguished as three different regions. Region A (that has the major area), characterized by strip-like 90° domain walls, corresponds to the tetragonal phase.[22] Those regions which exhibit optically isotropic background color, as indicated by arrows in Fig. 6(b), possibly correspond to rhombohedral clusters with the extinction directions along ⟨110⟩.[21] Thus, regions B and C, which exhibit complex interference patterns with unsharp domain walls, possibly correspond to rhombohedral clusters. PMN-34%PT shows similar domain structures with a mixture of two different states down to very low temperature (below 200 K). Upon heating, domain structures of the A region exhibit a sharp change near 445 K and this major volume of the PMN-34%PT crystal goes into the optically isotropic cubic state. However, residue of the 90° domain walls still can be seen in the region of 445–460 K. It may indicate that the internal stress requires higher temperature to release.

Different individual domain regions exhibit a large disparity not only in interference patterns, but also in transition temperatures. For instance, upon heating, the B and C regions of PMN-34%PT [Fig. 6(b)] exhibit a continuous change and go into the optically isotropic cubic phase near 438 K. But, strip-like 90° domain walls of A region show no apparent change up to ~445 K. Since the MPB depends sensitively on the relative Ti^{4+} occupancy on the *B* site, these phenomena suggest an inhomogeneous distribution of

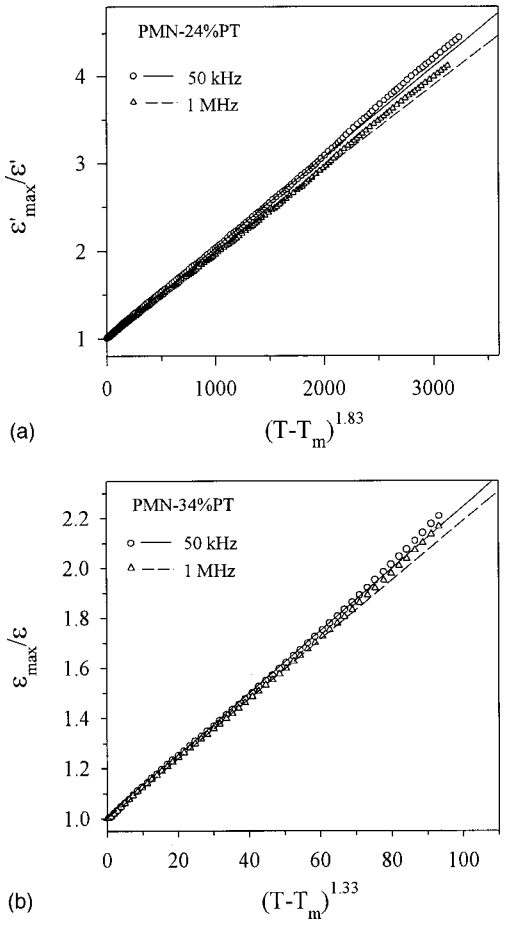

FIG. 8. $\varepsilon'_m/\varepsilon'$ vs $(T-T_m)^{\gamma}$ for (a) PMN-24%PT and (b) PMN-34%PT at measuring frequencies of 50 kHz and 1 MHz.

the Ti^{4+} concentration in the crystal. Physical analysis by the JEOL 6100 electron microscope has revealed inhomogeneity of the local composition for the *B* site ions Mg^{2+}, Nb^{5+}, and Ti^{4+}. In the PMN-34%PT platelet that we measured, the Ti^{4+} concentration varies about ±3% from its nominal or average composition. Such a fluctuation is believed to result from a quenched unequal occupation of the *B* site by the competitive ions Mg^{2+}, Nb^{5+}, and Ti^{4+}. By micro-Brillouin scattering, the spatial microheterogeneity was also detected in the PMN-35%PT crystal.[28]

IV. DISCUSSION

A. PMN-24%PT

What are the physical origins of the temperature-dependent anomalies shown in Figs. 1(a)–6(a) for PMN-24%PT? The dielectric permittivity ε' [Fig. 1(a)] exhibits broad frequency-dependent behavior with maxima located near 380 K. The value of T_m is quite consistent with the temperature $\sim 385 \pm 5$ K (cubic PE↔rhombohedral FE) predicated in Ref. 7. As the temperature increases, the acoustic phonon frequency [Fig. 2(a)] shows a gradual softening and reaches a weak minimum near 380 K, indicating a so-called diffuse phase transition. Similar acoustic and dielectric anomalies were seen in pure PMN.[29] In addition, the phonon damping of PMN-24%PT exhibits gradual growth

TABLE I. Parameters from the fits of Eq. (1) to the dielectric permittivity ε' (above T_m).

	γ	δ_γ (50 kHz)	δ_γ (1 MHz)
PMN-24%PT	1.83	21.7	22.8
PMN-34%PT	1.33	6.34	6.49

with a broad maximum located near 380 K. Such a damping anomaly reveals that order parameter fluctuations are the dominant dynamic mechanism in the vicinity of a diffuse phase transition.

Ye and Dong recently examined domain morphology in flux-grown PMN-PT single crystals with 20%, 35%, and 50% Ti by polarized light microscopy.[21] At room temperature, the 20% Ti crystal had only a rhombohedral cluster.[21] According to the MPB of PMN-PT system,[7] both 20%PT and 24%PT compounds have only rhombohedral phase near room temperature. As revealed in Fig. 6(a), the PMN-24%PT crystal gradually transforms into the macroscopically cubic phase and is fully converted to the cubic phase near 375 K, indicating coexistence of rhombohedral and cubic phases in a wide temperature range. It is believed that the diffuse phase transition near 380 K, seen in Figs. 1(a) and 2(a), reflects the strongly local structural fluctuations between cubic PE and rhombohedral FE clusters.

Probably the most convincing evidence for the FE nature of PMN-24%PT is the extra peak in the zero-field-heated dielectric permittivity seen after field cooling in a dc bias field ($E=6$ kV/cm) to the domain state, shown in Fig. 7. The coercive field E_c is less than 4 kV/cm in the temperature range measured. An extra peak superimposed on the broad background of the dielectric permittivity is clearly evident at 370 K. The temperature for this anomaly (but not its amplitude) is independent of frequency. A similar field-induced dielectric anomaly was observed in the PMN system.[3,30] By heating the PMN crystal in a dc electric field, a long-range FE phase transition associated with an extra dielectric peak at $T_c \sim 212$ K was found.[3] It was concluded that the peak at $T_c \sim 212$ K in PMN is connected to the percolating polar cluster due to the suppression of the random fields originating from charged compositional fluctuations at the B site.[3] It is well known that in relaxor ferroelectrics the highly sensitive local polar clusters are easily affected by external perturbations, contrary to normal ferroelectrics; an external electric field may enhance the interactions between local polar microclusters and induces marked changes.[4,31] Thus, it is reasonable to expect that the extra peak at 370 K in the FC-ZFH dielectric permittivity (Fig. 7) is attributed to the establishment of the long-range percolating FE cluster during the FC process. In addition, the broad dispersive permittivity peak following FC has magnitude of 14 000 (Fig. 7), about 10% lower than the 15 500 value shown in Fig. 1(a) for ZFC. Perhaps the FC process induces domain reorientations, hence reduces the domain wall contributions to the dielectric permittivity. Another possibility is that this reduction could be a consequence of partial poling of the network of nonpercolating FE clusters by the external electric field. Additional information concerning the FE nature of PMN-24%PT is obtained from $P-E$ hysteresis loops. As shown in Fig. 5(a), a step-like discontinuity in P_r was observed near 370 K.

B. PMN-34%PT

For a normal FE phase transition, the transition temperature occurs near where the acoustic phonon frequency has a discontinuous change.[23] In PMN-34%PT, the acoustic phonon frequency has an irregular minimum near 445 K. Correspondingly, a sharp damping maximum [Fig. 2(b)] which could possibly be associated with the Landau–Khalatnikov-like maximum was also detected near 445 K. Such a damping anomaly is usually related to rapid growth of a long-range FE cluster.[29] The real part ε' of the dielectric permittivity exhibits a sharp change near 445 K. This value is quite consistent with the transition temperature 435 ± 5 K (cubic PE$\leftrightarrow$tetragonal FE) predicated in Ref. 7. In addition, a clear thermal hysteresis exists in the temperature region of $\sim 380\ \mathrm{K} < T < \sim 460\ \mathrm{K}$, indicating a metastable state near the phase transition temperature. Domain structures [Fig. 6(b)] also reveal that the PMN-34%PT crystal turns into the cubic region above 445 K. Thus, PMN-34%PT possesses a nearly normal first-order phase transition at $T_c \sim 445$ K from the tetragonal FE to the cubic PE phase.

Near room temperature, as shown in Fig. 1(b), the dielectric permittivity ε' of PMN-34%PT exhibits a gradual step down with a weak frequency dispersion. The imaginary part ε'' also shows complicated frequency dispersions in a wide temperature range. Correspondingly, the acoustic phonon frequency reaches a weak minimum near 280 K. A wide thermal hysteresis was observed below 360 K down to very low temperature. Domain structures [Fig. 6(b)] verify that both tetragonal and rhombohedral domains coexist from very low temperature (below 200 K) up to possibly $\sim$435 K. Recent domain morphology obtained by Ye and Dong confirmed that a flux-grown PMN-35%PT single crystal at room temperature had a mixture phase of tetragonal and rhombohedral domains.[21] Based on the above results, one can conclude that gradual-evolution anomalies of phonon frequency and dielectric permittivity near 280 K in PMN-34%PT are due to local structural fluctuations between rhombohedral and tetragonal clusters. We call this a first-order transition for two reasons. First, the thermal hysteresis in the dielectric permittivity shows that the system is metastable in this temperature region. Metastability can occur for first-but not second-order transitions.[23] Second, the point groups of the tetragonal and rhombohedral symmetries do not have a group–subgroup relation, so a transition between these phases must be of first order. The usual distinctions between first-and second-order transitions, such as discontinuity in dP/dT, do not apply for diffuse phase transitions.

To characterize the temperature dependence of the dielectric permittivity ε' above T_m, we fitted the experimental data to the empirical formula,[32–34]

$$\frac{\varepsilon'_m}{\varepsilon'(f,T)} = 1 + \frac{[T - T_m(f)]^\gamma}{2\delta_\gamma^2}, \tag{1}$$

where ε'_m corresponds to the maximum value of the dielectric permittivity at T_m. The value of $\gamma(1 \leqslant \gamma \leqslant 2)$ is the expression of the degree of dielectric relaxation in a relaxor-based FE material. When $\gamma=1$, Eq. (1) expresses Curie–Weiss behavior, while for $\gamma=2$, Eq. (1) is identical to Smolensky's formula that can be used to fit well the dielectric permitivity of PMN above T_m.[35,36] The parameter δ_γ has been used as a measure of degree of diffuseness for the diffuse phase transition in relaxor-based ferroelectrics.[33] Based on Eq. (1), δ_γ can be determined from the slope of $\varepsilon'_m/\varepsilon'$ vs $(T-T_m)^\gamma$, which is linear. Figures 8(a) and 8(b) show the plots of $\varepsilon'_m/\varepsilon'$ vs $(T-T_m)^\gamma$. The solid and dashed lines are the best fits of Eq. (1) to the dielectric data obtained at 50 kHz and 1 MHz, respectively. The fitting values of parameters are given in Table I. It was found that the experimental data in the temperature regions ($T_m \leqslant T \leqslant T_m+70$ K for PMN-24%PT and $T_m \leqslant T \leqslant T_m+25$ K for PMN-34%PT) obey empirical Eq. (1). The parameter δ_γ shows a weak tendency to change with frequency. Also, no correlation between the parameter γ and measuring frequency was found. Compared with PMN-34%PT, PMN-24%PT possesses bigger values of δ_γ and γ. In other words, PMN-24%PT has stronger degrees of diffuseness and relaxation behavior in the region of diffuse phase transition. However, at higher temperature regions ($T>T_m+70$ for PMN-24%PT and $T>T_m+25$ for PMN-34%PT), slight deviations from Eq. (1) were found in both crystals that could be attributed to the contribution of ionic conductivity activated by thermal energy. Bokov and Ye recently demonstrated that, in PMN and PMN-25%PT (ceramic sample), the dielectric permittivity γ' obeys the relation $\varepsilon'_A/\varepsilon' = 1+(T-T_A)^2/2\delta_A^2$ in a wide temperature range above T_m.[36] However, such an empirical quadratic law could not fit better than Eq. (1) in the dielectric data of PMN-24%PT and PMN-34%PT systems. We cannot explain this contradiction. The search to find a universal formula describing the temperature dependence of ε' in the vicinity of diffuse phase transition continues.

V. CONCLUSIONS

In PMN-24%PT, a coexistence of rhombohedral and cubic phases, which is characterized by the broad dielectric maximum and gradual evolution of the acoustic phonon, was observed in a wide temperature range. In other words, the PMN-24%PT crystal gradually transforms into the cubic phase and is fully converted to the cubic state above 375 K. In addition, the dielectric thermal hysteresis implies that the diffuse phase transition near 380 K is first-order type. The FC-ZFH dielectric result shows that an extra FE anomaly appears at 370 K, possibly due to the percolating polar cluster induced by an external electric field.

A nearly normal FE phase transition is seen near 445 K in PMN-34%PT. Near 280 K a weak diffused phase transition was observed and is attributed to local structural fluctuations between rhombohedral and tetragonal phases. The thermal hysteresis of the dielectric permittivity verifies that phase transitions near 280 and 445 K are, respectively, diffuse first order and first order. Besides, the dielectric permittivities of PMN-24%PT and PMN-34%PT obey the relation, $\varepsilon'_m/\varepsilon'(f,T) = 1+[T-T_m(f)]^\gamma/2\delta_\gamma^2$, in a wide temperature range above T_m.

ACKNOWLEDGMENTS

This work was supported by Grant No. NSC89-2112-M-030-006 (Republic of China) and DOD EPSCoR Grant No. N00014-99-1-0523.

[1] L. E. Cross, Ferroelectrics **76**, 241 (1987).
[2] D. Viehland, M. Wuttig, and L. E. Cross, Ferroelectrics **120**, 71 (1991).
[3] V. Westphal and W. Kleemann, and M. D. Glinchuk, Phys. Rev. Lett. **68**, 847 (1992).
[4] Z.-G. Ye, Key Eng. Mater. **155–156**, 81 (1998).
[5] L. A. Shebanov, P. Kaspostins, and J. Zvirgzds, Ferroelectrics **56**, 1057 (1984).
[6] M. L. Mulvihill, S. E. Park, G. Risch, Z. Li, and K. Uchino, Jpn. J. Appl. Phys., Part 1 **35**, 3984 (1996).
[7] T. R. Shrout, Z. P. Chang, N. Kim, and S. Markgraf, Ferroelectr. Lett. Sect. **12**, 63 (1990).
[8] D. S. Paik, S. E. Park, S. Wada, S. F. Liu, and T. R. Shrout, J. Appl. Phys. **85**, 1080 (1999).
[9] M. K. Durbin, E. W. Jacobs, J. C. Hicks, and S.-E. Park, Appl. Phys. Lett. **74**, 2848 (1999).
[10] U. Belegundu, X. H. Du, and K. Uchino, Ferroelectrics **222**, 67 (1999).
[11] S.-E. Park and T. R. Shrout, J. Appl. Phys. **82**, 1804 (1997).
[12] Y. Yamashita, Jpn. J. Appl. Phys., Part 1 **33**, 5328 (1994).
[13] S. W. Choi, T. R. Shrout, S. J. Jang, and A. S. Bhalla, Ferroelectrics **100**, 29 (1989).
[14] R. F. Service, Science **275**, 1878 (1997).
[15] H. Luo, G. Xu, P. Wang, and Z. Yin, Ferroelectrics **231**, 97 (1999).
[16] H. Fu and R. E. Cohen, Nature (London) **403**, 281 (2000).
[17] C.-S. Tu, F.-C. Chao, C.-H. Yeh, C.-L. Tsai, and V. H. Schmidt, Phys. Rev. B **60**, 6348 (1999).
[18] S. Gentil, G. Robert, N. Setter, P. Tissot, and J.-P. Rivera, Jpn. J. Appl. Phys., Part 1 **39**, 2732 (2000).
[19] M. K. Durbin, J. C. Hicks, S.-E. Park, and T. R. Shrout, J. Appl. Phys. **87**, 8159 (2000).
[20] S. Saitoh, T. Kobayashi, K. Harada, S. Shimanuki, and Y. Yamashita, Jpn. J. Appl. Phys., Part 1 **37**, 3053 (1998).
[21] Z.-G. Ye and M. Dong, J. Appl. Phys. **87**, 2312 (2000).
[22] F. Jona and G. Shirane, *Ferroelectric Crystals* (Dover, New York, 1993), Chap. IV, pp. 160–167.
[23] M. E. Lines and A. M. Glass, *Principles and Applications of Ferroelectrics and Related Materials* (Oxford, London, 1977).
[24] J. P. Remeika and A. M. Glass, MRS Bull. **5**, 37 (1970).
[25] E. C. Subbarao, Ferroelectrics **5**, 267 (1973).
[26] V. A. Bokov and I. E. Mylnikov, Sov. Phys. Solid State **3**, 613 (1961).
[27] Z.-G. Ye and H. Schmid, Ferroelectrics **145**, 83 (1993).
[28] F. M. Jiang and S. Kojima, Appl. Phys. Lett. **77**, 1271 (2000).
[29] C.-S. Tu, V. H. Schmidt, and I. G. Siny, J. Appl. Phys. **78**, 5665 (1995).
[30] R. Sommer, N. K. Yushin, and J. J. van der Klink, Phys. Rev. B **48**, 13230 (1993).
[31] O. Bidault, M. Licheron, E. Husson, G. Calvarin, and A. Morell, Solid State Commun. **98**, 765 (1996).
[32] H. T. Martirena and J. C. Burfoot, Ferroelectrics **7**, 151 (1974).
[33] Z. Y. Cheng, R. S. Katiyar, X. Yao, and A. Guo, Phys. Rev. B **55**, 8165 (1997).
[34] K. Uchino and S. Nomura, Ferroelectr. Lett. Sect. **44**, 55 (1982).
[35] G. A. Smolensky, J. Phys. Soc. Jpn. Suppl. **28**, 26 (1970).
[36] A. A. Bokov and Z.-G. Ye, Solid State Commun. **116**, 105 (2000); Appl. Phys. Lett. **77**, 1888 (2000).